

Article

Supported ultrafine NiCo bimetallic alloy nanoparticles derived from bimetal-organic frameworks: a highly active catalyst for furfuryl alcohol hydrogenation

Huanjun Wang, Xiaodan Li, Xiaocheng Lan, and Tiefeng Wang

ACS Catal., Just Accepted Manuscript • DOI: 10.1021/acscatal.7b03795 • Publication Date (Web): 19 Jan 2018

Downloaded from <http://pubs.acs.org> on January 19, 2018

Just Accepted

“Just Accepted” manuscripts have been peer-reviewed and accepted for publication. They are posted online prior to technical editing, formatting for publication and author proofing. The American Chemical Society provides “Just Accepted” as a free service to the research community to expedite the dissemination of scientific material as soon as possible after acceptance. “Just Accepted” manuscripts appear in full in PDF format accompanied by an HTML abstract. “Just Accepted” manuscripts have been fully peer reviewed, but should not be considered the official version of record. They are accessible to all readers and citable by the Digital Object Identifier (DOI®). “Just Accepted” is an optional service offered to authors. Therefore, the “Just Accepted” Web site may not include all articles that will be published in the journal. After a manuscript is technically edited and formatted, it will be removed from the “Just Accepted” Web site and published as an ASAP article. Note that technical editing may introduce minor changes to the manuscript text and/or graphics which could affect content, and all legal disclaimers and ethical guidelines that apply to the journal pertain. ACS cannot be held responsible for errors or consequences arising from the use of information contained in these “Just Accepted” manuscripts.



1
2
3
4
5
6
7 Supported ultrafine NiCo bimetallic alloy
8
9
10
11 nanoparticles derived from bimetal-organic
12
13
14
15 frameworks: a highly active catalyst for furfuryl
16
17
18
19 alcohol hydrogenation
20
21
22
23

24 *Huanjun Wang, Xiaodan Li, Xiaocheng Lan, Tiefeng Wang**
25
26

27
28 Beijing Key Laboratory of Green Reaction Engineering and Technology, Department of
29
30 Chemical Engineering, Tsinghua University, Beijing 100084, China.
31
32

33
34 **ABSTRACT:** Highly dispersed NiCo bimetallic alloy nanoparticles have been successfully
35
36 immobilized on the SiO₂ frameworks by using hetero-nuclear metal-organic frameworks (MOFs)
37
38 as metal alloy precursors. Catalyst characterizations revealed that the average size of NiCo alloy
39
40 particles was less than 1 nm, with a total metal loading of about 20 wt%. Compared with
41
42 individual Ni or Co MOF-derived catalysts and the catalysts prepared by the conventional
43
44 impregnation method, the ultrafine NiCo/SiO₂-MOF catalyst showed a much better catalytic
45
46 performance in the catalytic hydrogenation of furfuryl alcohol (FA) to tetrahydrofurfuryl alcohol
47
48 (THFA) under mild conditions, giving 99.8% conversion of FA and 99.1% selectivity to THFA.
49
50
51 It was found that a significant synergistic effect existed between Co and Ni within the
52
53
54
55
56
57
58
59
60

1
2
3 subnanometer NiCo/SiO₂-MOF catalyst, which was twice and 20 times more active than
4
5 Ni/SiO₂-MOF and Co/SiO₂-MOF, respectively.
6
7

8
9 **KEYWORDS:** NiCo bimetallic catalyst, subnanometer, metal-organic framework, furfuryl
10
11 alcohol, hydrogenation, tetrahydrofurfuryl alcohol
12
13

14 15 1. INTRODUCTION

16
17
18 Furfuryl alcohol (FA) is an important chemical derived from the hydrogenation of furfural, a
19
20 promising biomass platform compound produced by hydrolysis and dehydration of
21
22 hemicellulose.¹⁻² FA can be converted into various value-added chemicals, such as
23
24 tetrahydrofurfuryl alcohol (THFA),³⁻⁹ cyclopentanone,¹⁰ 2-methylfuran (2-MF),¹¹ 1,2-
25
26 pentanediol,¹²⁻¹³ 1,5-pentanediol¹³ and alkyl tetrahydrofurfuryl ether (ATE),¹⁴ by selective
27
28 hydrogenation, hydrogenolysis or etherification reactions. Among these reactions, the
29
30 hydrogenation of FA to THFA is of great importance, because THFA is not only a biodegradable
31
32 and environmentally benign furanic chemical with many agricultural and industrial applications,
33
34 but also a promising intermediate to prepare diols.¹⁵⁻¹⁷
35
36
37
38

39
40 Although a few examples of homogeneous catalysis have been reported in the literature for FA
41
42 hydrogenation,¹⁸ the difficult separation and loss of active components in homogeneous catalysis
43
44 make it necessary to develop the THFA production by heterogeneous catalysis. Group VIII (Ni,
45
46 Ru, Rh, Pd, Pt) metal catalysts are active for the hydrogenation of FA to THFA. Among non-
47
48 noble metals, Ni-based catalysts are most used for this reaction, which generally give a high
49
50 yield of THFA but need very harsh reaction conditions. Recently, some research groups reported
51
52 that supported noble metal catalysts showed good performance under mild conditions for FA
53
54 hydrogenation. For example, Khan et al. reported that metallic Ru nanoparticles intercalated in
55
56
57
58
59
60

1
2
3 hectorite catalyzed the hydrogenation of FA to THFA with a yield of 99% in methanol solvent at
4
5 40 °C and 2.0 MPa H₂.³ Yuan et al. showed that Pd supported on TiO₂ nanotubes had 98%
6
7 conversion of FA and 98% selectivity to THFA at room temperature and 0.1 MPa H₂.⁶ However,
8
9 the high price and low reserve of noble metals limit their applications, and it is desirable to
10
11 develop non-noble catalysts for FA hydrogenation under mild reaction conditions.
12
13

14
15 Metal-organic frameworks (MOFs) have attracted increasing attention due to their high surface
16
17 area, adjustable pore size and periodical skeletal structure. They have been widely investigated in
18
19 catalysis, gas storage and separation, ion exchange and chemical sensors.¹⁹⁻²⁰ More recently,
20
21 MOFs have also been demonstrated to be promising precursors and templates to fabricate porous
22
23 carbon,²¹⁻²⁴ metal oxides²⁵⁻²⁷ and other supported metal catalysts.²⁸ In particular, the
24
25 homogeneous component of multivariate MOFs with different metal centers provides an
26
27 opportunity to synthesize multivariate mixed-metal oxides or mixed-metal alloys.²⁹⁻³⁰ For
28
29 example, Chen et al. synthesized Ni_xCo_{3-x}O₄ nanoparticles for supercapacitors by calcination of
30
31 multivariate MOF-74.³¹ Long et al. synthesized multimetal-MOF-derived NiCo alloy
32
33 nanoparticles of 20.6 nm embedded in nitrogen-doped carbon matrix, which showed a high
34
35 transfer hydrogenation performance for nitriles.³² However, using bimetal-MOFs as precursors to
36
37 synthesize supported non-noble subnanometer-scale alloy nanoparticles has not been reported.
38
39
40
41
42
43

44
45 In this work, we reported successful synthesis of subnanometer-scale NiCo nanoparticles
46
47 immobilized on SiO₂ support using NiCo-MOF as precursor, which showed a very high activity
48
49 and good stability in the FA hydrogenation reaction under mild conditions. It was found that the
50
51 prepared subnanometer-scale NiCo nanoparticles supported on SiO₂ showed a strong bimetallic
52
53 synergistic effect on the catalytic hydrogenation of FA to THFA. This synergistic effect was
54
55
56
57
58
59
60

investigated by comparing with the individual Ni or Co MOF-derived catalysts and the impregnation catalysts, combining various characterization techniques.

2. EXPERIMENTAL SECTION

2.1 Materials

Furfuryl alcohol (FA, 98%) and sodium borohydride (NaBH_4 , purity > 98%) were purchased from J&K Scientific Ltd. Ionic liquids (ILs) 1-octyl-3-methylimidazolium perchlorate (OmimClO_4 , purity > 99%) and triethylammonium nitrate ($\text{N}(\text{C}_2\text{H}_5)_3\text{HNO}_3$, purity > 99%) were provided by the Centre of Green Chemistry and Catalysis, LICP, CAS. $\text{Ni}(\text{NO}_3)_2 \cdot 6\text{H}_2\text{O}$ (98%), $\text{Co}(\text{NO}_3)_2 \cdot 6\text{H}_2\text{O}$ (98%), tetraethoxysilane (TEOS, 99.9%) and silica (SiO_2 , 147 m^2/g) were purchased from Alfa Aesar. 1,3,5-benzenetricarboxylic acid (H_3BTC , 98%) was obtained from Acros Organics. *N,N*-Dimethylformamide (DMF, A. R. grade), acetone (A. R. grade) and ethanol (A. R. grade) were provided by Modern Oriental (Beijing) Technology Development Co. Ltd. All agents were used as received except that furfuryl alcohol was purified by vacuum distillation before use.

2.2 Synthesis of MOF-derived catalysts

The MOF-derived catalysts were denoted as $\text{M}/\text{SiO}_2\text{-MOF}$ ($\text{M} = \text{Ni}, \text{Co}$ and NiCo) and the synthetic method for the $\text{NiCo}/\text{SiO}_2\text{-MOF}$ catalyst was described as follows. In a typical synthesis,²⁸ 70 g OmimClO_4 , 25 g $\text{N}(\text{C}_2\text{H}_5)_3\text{HNO}_3$ and 30 g water were added to a 250 mL conical flask equipped with a condenser to form a homogeneous solution. Then the precursors of NiCo-MOF , 1.5 g $\text{Ni}(\text{NO}_3)_2 \cdot 6\text{H}_2\text{O}$, 1.5 g $\text{Co}(\text{NO}_3)_2 \cdot 6\text{H}_2\text{O}$, 3.0 g H_3BTC , and the precursor of SiO_2 , 6 mL TEOS, were introduced into the above solution at 80 °C. The mixture was stirred at

1
2
3 1000 rpm for 48 h, followed by aging at 80 °C for 24 h. Afterwards, the precipitate was separated
4
5 by centrifugation and washed three times with acetone. Finally, the precipitate was dried in a
6
7 vacuum drying oven at 40 °C for 24 h, and the NiCo-MOF/SiO₂ composite was obtained.
8
9

10
11 The prepared NiCo-MOF/SiO₂ was reduced by the liquid-phase method to synthesize the
12
13 supported ultrafine bimetal catalyst NiCo/SiO₂-MOF. In the experiment, 0.5 g NiCo-MOF/SiO₂
14
15 composite was dispersed into 80 mL 50 wt% DMF aqueous solution in a 250 mL three-necked
16
17 flask at 25 °C. Then 50 mL cold NaBH₄ DMF aqueous solution (10 g·L⁻¹) was added into the
18
19 mixture over 60 min under the protection of CO₂ with stirring, followed by further stirring for an
20
21 additional 3 h. After that, the mixture was separated by centrifugation at 4000 rpm and washed
22
23 with deionized water and ethanol three times. The obtained sample was dried in a vacuum drying
24
25 oven at 40 °C for 24 h to give the NiCo/SiO₂-MOF catalyst. The procedure to synthesize the
26
27 monometallic MOF-derived supported catalysts was similar. The main difference was that only
28
29 Ni(NO₃)₂·6H₂O or Co(NO₃)₂·6H₂O was used as the MOF precursors.
30
31
32
33
34

35 **2.3 Synthesis of M/SiO₂ catalysts by repeated impregnation method**

36
37

38 For comparison, the M/SiO₂ catalysts were prepared with the repeated incipient wetness
39
40 impregnation method and denoted as M/SiO₂-IMP (M = Ni, Co, and NiCo). Because the
41
42 solubility of the nitrates and the water absorption capacity of the supports were low, the catalysts
43
44 with high loadings could not be prepared in one impregnation. For NiCo/SiO₂-IMP, the desired
45
46 amount of Ni and Co nitrates were divided into four portions, and used to impregnate the support
47
48 four times. The procedures for each impregnation were as follows. First, the precursor solution
49
50 was prepared by dissolving a desired amount of Ni(NO₃)₂·6H₂O or Co(NO₃)₂·6H₂O in deionized
51
52 water just sufficient to fill the pores of 3.0 g SiO₂ support. Then the precursor solution was added
53
54
55
56
57
58
59
60

1
2
3 to the support dropwise and treated with ultrasound for 1 h to facilitate metal dispersion. After
4
5 aging in air at ambient temperature overnight, the catalyst was dried in air at 80 °C for 10 h and
6
7 calcined at 450 °C for 3 h. The catalyst obtained after four times of impregnation was stored in
8
9 vials and reduced under H₂ flow with a flow rate of 60 mL/min at 450 °C for 3 h prior to
10
11 catalytic evaluation. The procedure to synthesize the monometallic catalysts was similar except
12
13 that only one kind of nitrate was used.
14
15
16

17 18 **2.4 Materials characterization**

19
20
21 The X-ray diffraction (XRD) analysis was carried out on a Bruker D8 Advance powder X-ray
22
23 diffractometer (40 kV, 40 mA) with Cu K α ($\lambda = 1.5406 \text{ \AA}$) monochromatic radiation source in
24
25 the 2θ range of 5–90°, and the scan speed was 2 °/min. The surface area and porous structure
26
27 were measured using N₂ adsorption-desorption isotherms at 77 K with a Quantachrome autosorb
28
29 iQ and AsiQwin instrument. Before measurements, the samples were degassed under vacuum at
30
31 30 °C for 10 h. The Brunauer–Emmett–Teller (BET) and Barrett–Joyner–Halenda (BJH)
32
33 methods were used to calculate the specific surface area and pore sizes, respectively. The actual
34
35 loadings of Ni and Co on the catalysts were determined by a Spectro Arcos FHX22 inductively
36
37 coupled plasma optical emission spectrometer (ICP-OES). Scanning electron microscopy (SEM)
38
39 images were recorded on a JEOL JSM-7401F instrument. Transmission electron microscopy
40
41 (TEM) images and element mapping were collected on a JEOL JEM-2010 instrument operated at
42
43 120 kV with an energy dispersive X-ray (EDX) detector. High resolution TEM (HRTEM), high-
44
45 angle annular dark-field scanning TEM (HAADF-STEM) and element mapping were conducted
46
47 on a JEOL JEM-2100F instrument working at 200 kV. The X-ray photoelectron spectroscopy
48
49 (XPS) analysis was performed on a Thermal Scientific ESCALAB 250Xi instrument using an Al
50
51
52
53
54
55
56
57
58
59
60

1
2
3 $K\alpha$ X-ray source. A low-resolution survey and high-resolution region scans at the binding energy
4
5 of interest were collected for each sample.
6
7

8 9 **2.5 Catalytic evaluation**

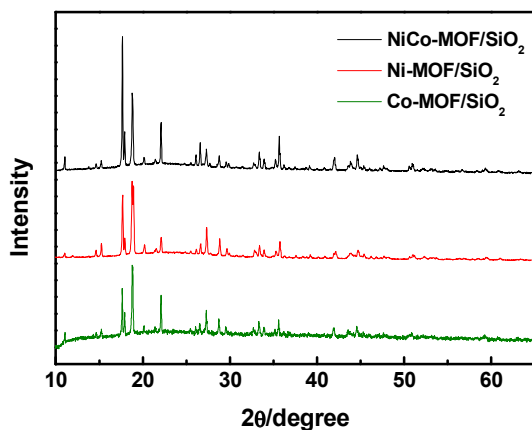
10
11
12 The selective hydrogenation of FA was carried out in a stainless steel autoclave (Weihai
13
14 Chemical Machinery Co., Ltd., 300 mL). In a typical experiment, 4.0 g purified FA, 100 mL
15
16 ethanol and 0.150 g catalyst were added to the reactor. After the reactor was sealed, the reaction
17
18 system was purged with 180 mL/min H_2 gas flow for 10 min at room temperature. Afterwards,
19
20 the reactor was heated to 80 °C under 0.5 MPa. When the temperature reached to 80 °C, the
21
22 pressure was increased from 0.5 to 3.0 MPa within 5 min. The time when the pressure reached
23
24 3.0 MPa was considered as the zero of reaction time. The pressure of the reaction system was
25
26 controlled by a back-pressure valve. The stirring speed was set at 800 rpm, and the H_2 flow rate
27
28 was set at 180 mL/min, which were found high enough to eliminate the gas-liquid mass transfer
29
30 resistance. The products were sampled and analyzed by a gas chromatograph (GC 7900 II,
31
32 Techcomp Instrument Company) equipped with a super-wax capillary column (30 m \times 0.25 mm
33
34 \times 0.5 μ m) and an FID detector. The products were identified by comparing with authentic
35
36 samples, and the reactant and products were quantified by external calibration.
37
38
39
40
41
42

43 **3. RESULTS AND DISCUSSION**

44 45 46 **3.1 Synthesis and characterization of the NiCo-MOF/SiO₂ precursor**

47
48
49 As shown by XRD patterns in Figure 1, the NiCo-MOF/SiO₂ composite had similar diffraction
50
51 peaks to those of the monometallic Ni-MOF/SiO₂ and Co-MOF/SiO₂ composites, indicating that
52
53 these composites had similar crystal structure. Furthermore, all peaks of the three composites
54
55
56
57
58
59
60

1
2
3 matched well with those of the reported bulk phase of $\text{Ni}_3(\text{BTC})_2 \cdot 12\text{H}_2\text{O}$ (Ni-MOF) and
4
5 $\text{Co}_3(\text{BTC})_2 \cdot 12\text{H}_2\text{O}$ (Co-MOF),³³ confirming the successful synthesis of various MOFs.
6
7
8
9



25 **Figure 1.** Powder XRD patterns of NiCo-MOF/SiO₂, Ni-MOF/SiO₂ and Co-MOF/SiO₂.

26
27
28 The N₂ adsorption-desorption isotherms of NiCo-MOF/SiO₂ and corresponding pore size
29 distribution are shown in Figures 2a and 2b, respectively. The isotherms of NiCo-MOF/SiO₂
30 could be categorized as type IV with H₃ hysteresis loop, in accordance with mesoporous
31 materials. The pore size distribution had a peak centered at 10.1 nm. The BET surface area and
32 pore volume were 190 m²/g and 0.62 cm³/g, respectively. The N₂ adsorption-desorption
33 isotherms and mesopore size distributions of Ni-MOF/SiO₂ and Co-MOF/SiO₂ are shown in
34 Figure S1. The BET surface area, total pore volume and average pore size of these three
35 composites are listed in Table S1. As revealed by Figure S1 and Table S1, the Ni-MOF/SiO₂ and
36 Co-MOF/SiO₂ composites showed mesoporous characteristics similar to the NiCo-MOF/SiO₂
37 composite.
38
39
40
41
42
43
44
45
46
47
48
49
50
51
52
53
54
55
56
57
58
59
60

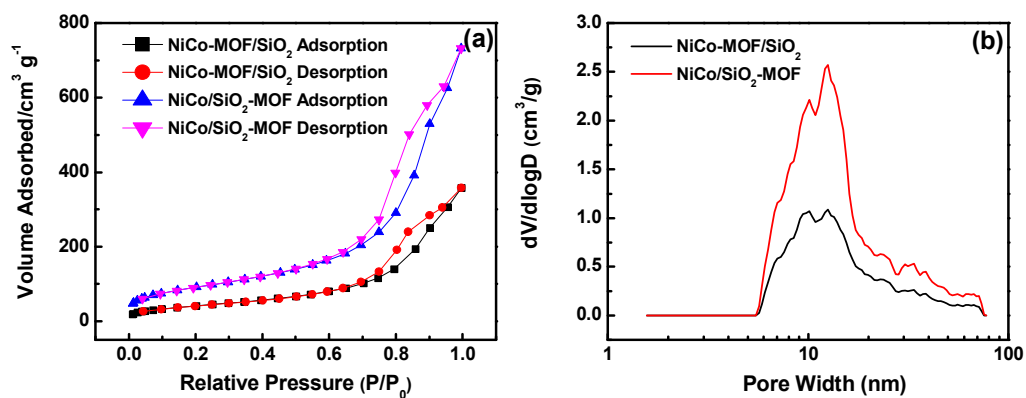


Figure 2. (a) N₂ adsorption-desorption isotherms and (b) mesopore size distribution of NiCo-MOF/SiO₂ and NiCo/SiO₂-MOF.

The surface morphology of the NiCo-MOF/SiO₂ composite was investigated by SEM. As shown in Figure 3a, the as-synthesized NiCo-MOF/SiO₂ composite was a mixture of NiCo-MOF and amorphous SiO₂. The NiCo-MOF particles, which had smooth surfaces and were made of fragments of rectangular bars of ~2 μm in size, were mainly trapped in the SiO₂ framework. The SiO₂ support had a loose and porous morphology, consistent with the BET results. The SEM images of Ni-MOF/SiO₂ and Co-MOF/SiO₂ are shown in Figure S2, indicating that these two composites were also mixtures of MOF and amorphous SiO₂. The TEM image of the NiCo-MOF/SiO₂ composite and the corresponding elemental mapping results are shown in Figures 3b and 3c, respectively, indicating a highly uniform distribution of Ni, Co and O in NiCo-MOF surrounded by the SiO₂ framework and confirming the successful formation of hetero-dinuclear MOFs rather than physical mixing of monometallic MOFs.

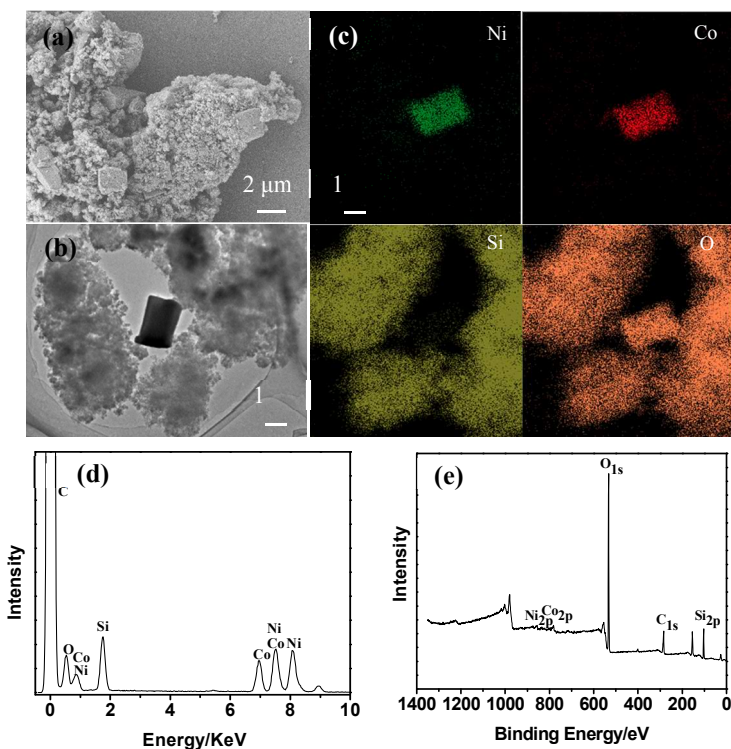


Figure 3. Related characterizations of NiCo-MOF/SiO₂ composite: (a) SEM image, (b) TEM image and (c) corresponding elemental mapping for Ni, Co, Si, O, (d) EDS spectrum and (e) XPS survey spectrum.

The EDS results of NiCo-MOF/SiO₂ are shown in Figure 3d. The peaks of C, O, Co, Ni and Si agreed well with the composition of NiCo-MOF/SiO₂, which further confirmed the successful formation of bimetal-MOF composites. The chemical composition of NiCo-MOF/SiO₂ was measured by XPS. As shown in Figure 3e, the full-survey-scan spectrum has five dominant peaks at 103.8, 284.8, 533.1, 781.5 and 856.1 eV corresponding to Si 2p, C 1s, O 1s, Co 2p and Ni 2p, respectively, consistent with the EDS results. The Ni and Co loadings in NiCo-MOF/SiO₂ determined by ICP-OES were 6.6 wt% and 6.9 wt%, respectively, which agreed well with the dosage of metal salts. All these characterizations indicated the successful formation of NiCo-MOF in the SiO₂ frameworks.

3.2 Synthesis and characterization of the NiCo/SiO₂-MOF catalyst

After liquid-phase reduction, the organic ligands in the MOF were dissolved in the DMF aqueous solution and the reduced metal nodes were immobilized on SiO₂. The actual metal loading in the final catalysts were measured by ICP-OES, as listed in Table 1. The overall metal loading of MOF-derived catalyst was around 20 wt% (Table 1, entry 1-3). For comparison, we also synthesized the SiO₂ supported Ni, Co and NiCo catalysts with a total metal loading of 20 wt% using the repeated impregnation method.

Table 1. Metal loading, BET surface area (S), total pore volume (V_p), average mesopore diameter (D_{pore}) and the average particle size ($D_{particle}$) of different catalysts.

Entry	Catalysts	Metal loading/wt%		S m ² ·g ⁻¹	V_p cm ³ ·g ⁻¹	D_{pore} nm	$D_{particle}$ nm
		Ni	Co				
1	NiCo/SiO ₂ -MOF	10.3	10.5	340	1.07	12.6	<1
2	Ni/SiO ₂ -MOF	17.0	/	347	1.05	10.1	<1
3	Co/SiO ₂ -MOF	/	19.9	445	1.12	10.1	<1
4	NiCo/SiO ₂ -IMP	10.0	10.0	114	0.40	12.6	14.3
5	Ni/SiO ₂ -IMP	20.0	/	118	0.46	12.1	12.0
6	Co/SiO ₂ -IMP	/	20.0	124	0.45	12.6	12.7

The XRD patterns of different catalysts are shown in Figure 4. All the catalysts had a diffraction peak at 21.98°, which was the characteristic peak of SiO₂. For the Ni/SiO₂-IMP catalyst, three peaks centered at 44.47°, 51.85° and 76.34° were found, which could be assigned to (111), (200) and (220) of face-centered cubic (fcc) nickel, respectively. No signals of nickel hydroxide or nickel oxide were observed. The XRD pattern of Co/SiO₂-IMP had three peaks at 44.33°, 51.57°

and 75.89° , corresponding to (111), (200) and (220) of fcc cobalt, respectively. For NiCo/SiO₂-IMP, the XRD peaks occurred at 44.44° , 51.72° and 76.30° , similar to those of either fcc Ni or fcc Co. Slight variations in the peak position were observed and all the peaks lied between those of pure fcc Ni and Co, confirming the formation of Ni-Co alloy.³⁴ The characteristic peaks of Ni, Co and NiCo for the three catalysts synthesized by impregnation are sharp, indicating high crystallinity and large particle sizes. However, except the peak at 21.98° for SiO₂, the XRD patterns of the three MOF-derived catalysts had only one broad peak at around 44.5° , indicating very small metal particles supported on SiO₂.

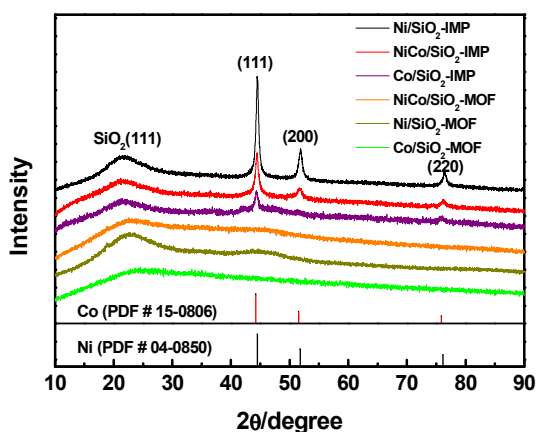


Figure 4. Powder XRD patterns of various catalysts.

To investigate the BET surface area and pore size of the NiCo/SiO₂-MOF catalyst, N₂ adsorption-desorption measurements were performed. As shown in Figure 2a, the N₂ adsorption amount of the NiCo/SiO₂-MOF catalyst was higher than that of the NiCo-MOF/SiO₂ precursor, indicating that NiCo/SiO₂-MOF had a bigger surface area. The pore size distribution remained almost unchanged before and after reduction, but the total pore volume became larger, ascribing to the organic ligands removal of NiCo-MOF particles trapped in the SiO₂ framework, as shown

1
2
3 in Figure 2b. The N₂ adsorption-desorption isotherms and pore size distribution curves of the
4 monometallic MOF-derived catalysts were similar to those of NiCo/SiO₂-MOF, as shown in
5 Figure S3. The BET surface area, total pore volume and average pore size of all catalysts are
6 listed in Table 1. Compared with the impregnation catalysts, the MOF-derived catalysts had
7 bigger BET surface area and larger total pore volume (Table 1 and Figure S4), which was
8 attributed to the removal of organic ligands.
9

10
11
12 The microstructure of the NiCo/SiO₂-MOF catalyst was further characterized by TEM
13 measurements. The bright-field HRTEM image (Figure 5a) showed that the tiny NiCo
14 nanoparticles were highly dispersed on the SiO₂ support and had a narrow size distribution of 0.6
15 ± 0.2 nm, as shown in Figure 5b. The HAADF-STEM and corresponding element mapping
16 analyses were performed to detect the element distribution in the NiCo/SiO₂-MOF catalyst. As
17 shown in Figures 5c and 5d, the element distribution of Ni and Co in this catalyst obviously
18 overlapped, further confirming that NiCo alloy nanoparticles were highly dispersed on the SiO₂
19 support. Because the metal particles of NiCo alloy were very small, it was difficult to identify the
20 exact composition of an individual particle. We performed EDS analyses of three small regions
21 enclosed with circles during the HAADF-STEM observation, as shown in Figures 5e and 5f. It
22 was found that the characteristic peaks of Ni and Co appeared simultaneously in all three
23 regions, suggesting that bimetallic alloy particles were formed on the SiO₂ support. The HRTEM
24 images and particle size distribution of the monometallic MOF-derived catalysts and
25 impregnation catalysts are shown in Figures S5 and S6, respectively. The particle sizes of both
26 Ni/SiO₂-MOF and Co/SiO₂-MOF were less than 1 nm, whereas the average particle sizes of the
27 impregnation catalysts were larger than 10 nm, being 14.3, 12.0 and 12.7 nm for NiCo/SiO₂-
28 IMP, Ni/SiO₂-IMP and Co/SiO₂-IMP, respectively.
29
30
31
32
33
34
35
36
37
38
39
40
41
42
43
44
45
46
47
48
49
50
51
52
53
54
55
56
57
58
59
60

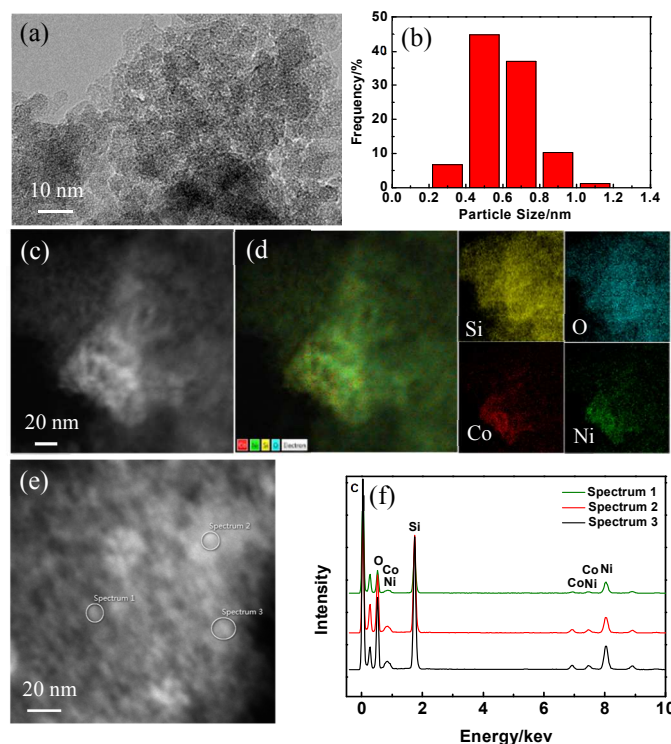


Figure 5. Related morphology characterization of the NiCo/SiO₂-MOF catalyst: (a) HRTEM image and (b) corresponding particle size distribution; (c) HAADF-STEM image and (d) corresponding EDS layered image, and element mappings for Si, O, Co, Ni; (e) HAADF-STEM image and (f) corresponding EDS profiles for different regions enclosed with three circles.

The chemical states of the NiCo/SiO₂-MOF catalyst were measured by XPS analysis. The green line in Figure 6a shows that the Ni 2p peak splits at 856.28 and 874.03 eV in a 2:1 peak area ratio, which are assigned to the characteristics of 2p_{3/2} and 2p_{1/2} levels of Ni²⁺ in NiCo-MOF, respectively.³⁵⁻³⁶ Moreover, two shake-up peaks at the high binding energy side to the main lines were detected. These satellite peaks are characteristic of Ni²⁺ oxidation state.³⁷ After reduction, the red line in Figure 6a shows that the Ni 2p_{3/2} of the NiCo/SiO₂-MOF catalyst is deconvoluted into two main peaks at 855.99 and 852.40 eV, which are assigned to Ni(OH)₂ and Ni⁰,

respectively. The peak area ratio between Ni⁰ and Ni(OH)₂ was 27:73, indicating that nickel was mainly present in an oxidation state because the smaller particles were more easily oxidized.

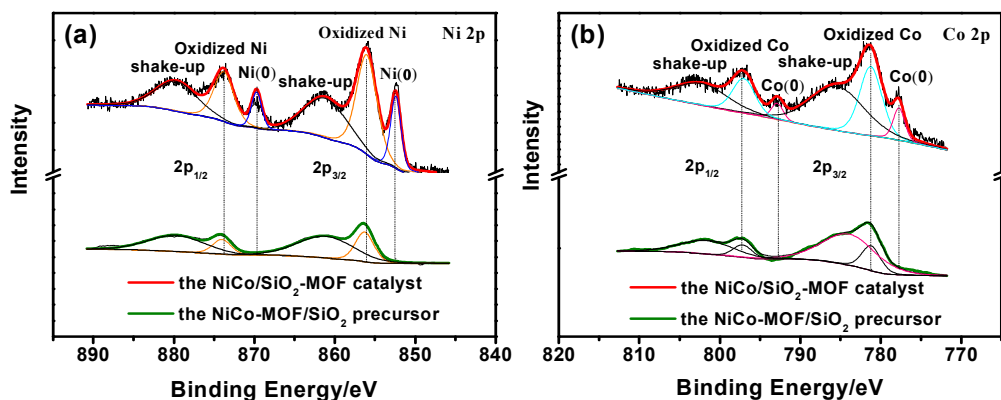


Figure 6. XPS spectrum of MOF-derived bimetallic NiCo catalyst before and after reduction: (a) Ni 2p and (b) Co 2p. Reduction conditions: 0.5 g NiCo-MOF/SiO₂ composite, 80 mL 50 wt% DMF aqueous solution as solvent, 50 mL NaBH₄ DMF aqueous solution (10 g·L⁻¹) as reductant, 25 °C, 0.1 MPa CO₂ and TOS = 4 h.

Similarly, the Co 2p spectrum of NiCo-MOF/SiO₂ (the green line in Figure 6b) also exhibits two contributions at 781.25 and 797.22 eV with two shake-up peaks at high binding energy, which are assigned to 2p_{3/2} and 2p_{1/2} levels of Co²⁺ in NiCo-MOF, respectively. After reduction, the Co 2p spectrum of the NiCo/SiO₂-MOF catalyst (the red line in Figure 6b), which is fitted by considering two resolved doublets, clearly evidences the presence of two chemical environments for surface Co atoms. The first predominant doublet, present at 781.25 eV (2p_{3/2}) and 797.03 eV (2p_{1/2}), is characteristic of Co²⁺ oxidation state. The second one with a lower intensity is located at lower binding energies, 777.74 eV (2p_{3/2}) and 792.87 eV (2p_{1/2}), corresponding to cobalt in metallic state.³⁸ The peak area ratio between Co⁰ and Co²⁺ was 20:80, indicating that most of

cobalt was in an oxidation state. As shown in Table S2, the ratio of metal state Ni to oxidation state Ni in the NiCo/SiO₂-MOF catalyst is higher than that in the Ni/SiO₂-MOF. The reason was that preferential oxidation of Co occurred because the Gibbs free energy of Co oxides formation is lower than that of Ni oxides.³⁹⁻⁴⁰ The wide survey XPS spectrum of the NiCo/SiO₂-MOF catalyst revealed that the surface atomic ratio between Ni and Co was 66:34, which was higher than the ICP measured value 49:51, implying that the Ni element in the NiCo/SiO₂-MOF catalyst was mainly located at the surface of the catalyst.

3.3 Catalytic evaluation of NiCo/SiO₂-MOF

A series of experiments were designed to study the catalytic performance of the NiCo/SiO₂-MOF catalyst for FA hydrogenation to THFA under liquid-phase conditions. The results are summarized in Table 2 and Figures 7, 8. Typically, the reactions were performed at 80 °C and 3.0 MPa H₂ atmosphere in a batch reactor. It is worth noting that the solvent plays an essential role in the hydrogenation activity.⁴¹ Considering that alcohols have a better H₂ solubility and can stabilize the reactive intermediates of this reaction,⁶ we used ethanol as the solvent.

Table 2. Catalytic performances of different catalysts for furfuryl alcohol hydrogenation to tetrahydrofurfuryl alcohol.^a

Entry	Catalysts	Conversion (%)	Selectivity (%)		k_r (10 ⁻⁴ min ⁻¹)
			THFA	Others ^b	
1	NiCo/SiO ₂ -MOF	99.8	99.1	0.9	124.7
2	Ni/SiO ₂ -MOF	96.9	95.3	4.7	63.8
3	Co/SiO ₂ -MOF	28.1	50.1	49.9	6.3
4	NiCo/SiO ₂ -IMP	73.0	92.9	7.1	27.1

5	Ni/SiO ₂ -IMP	90.6	97.6	2.4	47.8
6	Co/SiO ₂ -IMP	21.9	60.1	39.9	4.9

^a Reaction conditions: 4.0 g furfuryl alcohol, 100 mL ethanol as solvent, 0.150 g catalyst, 80 °C, 3.0 MPa H₂ and TOS = 8 h. ^b Side-products were the intermediates of partial-hydrogenation of one C=C bond in the furan ring and traces of 1,5-pentanediol.

For better comparison, we also evaluated the Ni/SiO₂-MOF and Co/SiO₂-MOF catalysts with a similar total metal loading. As shown in Table 2 and Figure 7a, the NiCo/SiO₂-MOF catalyst has the best catalytic performance, with 99.8% conversion of FA and 99.1% selectivity to THFA after 8 h of reaction (Table 2, entry 1). The catalyst activity and selectivity followed a trend of NiCo/SiO₂-MOF > Ni/SiO₂-MOF > Co/SiO₂-MOF. The plots of $-\ln(1-X)$ as a function of reaction time are straight lines passing through the origin (Figure 7b), indicating that the reaction is pseudo first-order with respect to FA. The calculated rate constants for NiCo/SiO₂-MOF, Ni/SiO₂-MOF and Co/SiO₂-MOF are 124.7, 63.8 and 6.3×10^{-4} min⁻¹ (Table 2, entry 1-3), respectively. The rate constant of NiCo/SiO₂-MOF is about twice higher than Ni/SiO₂-MOF, and 20 times higher than Co/SiO₂-MOF, showing a significant synergistic effect between Co and Ni. As revealed by the XPS results, alloying Co with Ni has a profound effect on the oxidation state of Ni and the abundance of surface Ni species, which not only suppresses the oxidation of Ni, but also enhances the content of Ni on the surface of the catalyst.

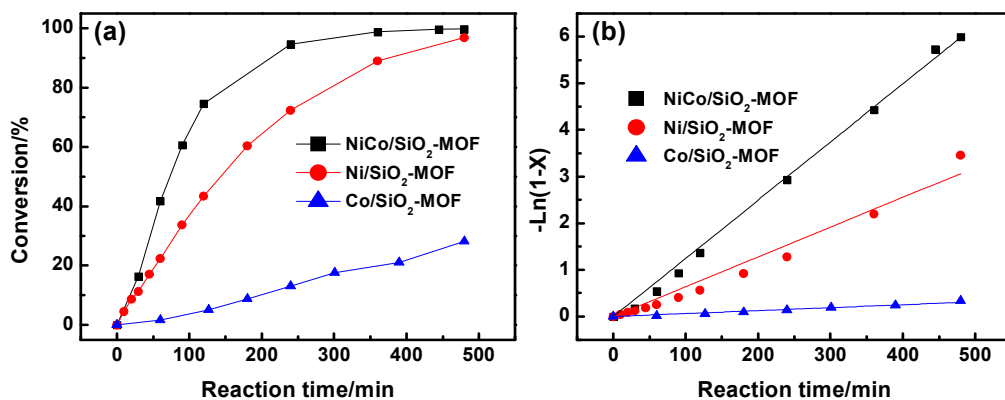


Figure 7. Comparison of monometallic and bimetallic Ni and Co MOF-derived catalysts: (a) Conversion vs. reaction time and (b) $-\ln(1-X)$ vs. reaction time for hydrogenation of FA. Reaction conditions: 4.0 g furfuryl alcohol, 100 mL ethanol as solvent, 0.150 g catalyst, 80 °C, 3.0 MPa H₂ and TOS = 8 h.

To further evaluate the catalytic performance of NiCo/SiO₂-MOF, we also performed the reactions using the catalysts prepared by impregnation. As shown in Table 2 and Figure 8, among the three impregnation catalysts, the Ni/SiO₂-IMP catalyst has the best catalytic performance, with a rate constant of $47.8 \times 10^{-4} \text{ min}^{-1}$ and 97.6% selectivity to THFA (Table 2, entry 5). The Co/SiO₂-IMP catalyst has the lowest rate constant of $4.9 \times 10^{-4} \text{ min}^{-1}$ and only 60.1% selectivity to THFA (Table 2, entry 6). Different from the MOF-derived catalysts, the bimetallic NiCo/SiO₂-IMP catalyst shows a moderate activity, with a rate constant of $27.1 \times 10^{-4} \text{ min}^{-1}$ and 92.9% selectivity to THFA (Table 2, entry 4). Among all the catalysts studied in this work, the NiCo/SiO₂-MOF catalyst has the best catalytic performance with 99.8% conversion of FA and 99.1% selectivity to THFA (Table 2, entry 1), which was mainly ascribed to the subnanometer size of metal particles and bimetallic effect.

The excellent catalytic performance of NiCo/SiO₂-MOF can be attributed to the following aspects. First, the ultrafine metal alloy nanoparticles offer more active sites than the large NiCo particles prepared by impregnation, thus giving a higher activity for FA hydrogenation. Second, the synergistic effect between Ni and Co in ultrafine NiCo alloy particles suppresses the oxidation of Ni, contributing to a higher activity of NiCo/SiO₂-MOF than its monometallic counterparts. Third, the removal of organic ligands during the liquid-phase reduction increases the total pore volume and surface area, which benefits for reactants adsorption and internal diffusion. This highly active catalyst has great potential applications in conversion of other biomass-derived platform compounds. In addition, the significant bimetallic synergistic effect of the subnanometer-scale NiCo alloy catalyst reveals that nanoclusters exhibit novel properties that differ greatly from those predicted by simple scaling laws, which provides new opportunity for developing high-performance catalysts.

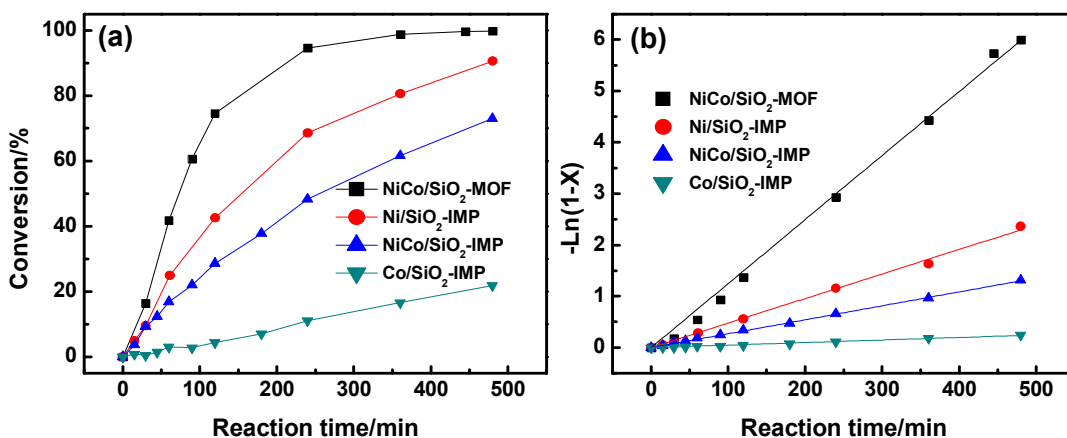


Figure 8. Comparison of monometallic and bimetallic Ni and Co impregnation catalysts: (a) Conversion vs. reaction time and (b) $-\ln(1-X)$ vs. reaction time for hydrogenation of FA. Reaction conditions are the same as in Figure 7.

1
2
3 The reusability of NiCo/SiO₂-MOF was investigated by recycling experiments. After reactions,
4 the reaction solution was centrifuged to separate the catalyst. The collected catalyst was washed
5 with ethanol, dried under vacuum, and then reused in the next reaction cycle. Five consecutive
6 runs were conducted. The conversion of FA and the selectivity to THFA after 8 h are shown in
7 Figure S8. The NiCo/SiO₂-MOF catalyst maintains high conversion and selectivity in the five
8 consecutive runs with only slight decrease in activity. The XRD pattern and TEM images of the
9 spent catalyst are shown in Figure S9 and S10, respectively. It can be seen that the crystal
10 structure is maintained as determined by XRD analysis, and the size of NiCo nanoparticles on
11 the spent catalyst is nearly the same as that of the fresh catalyst as shown by TEM images. ICP-
12 OES analysis further reveals that the leaching loss in the NiCo/SiO₂-MOF catalyst after five runs
13 is only 1.0 wt% for Ni and 1.3 wt% for Co, indicating that the NiCo/SiO₂-MOF catalyst has a
14 reasonable stability in FA hydrogenation to THFA.
15
16
17
18
19
20
21
22
23
24
25
26
27
28
29
30

31 **4. CONCLUSIONS**

32
33
34
35 We have developed a novel and facile method to prepare ultrafine NiCo bimetallic alloy
36 nanoparticles supported on porous SiO₂ by reducing hetero-dinuclear MOFs. Catalyst
37 characterizations reveal that bimetallic MOF-derived NiCo alloy NPs less than 1 nm are highly
38 dispersed on the porous SiO₂ support with a total metal loading of about 20 wt%. The
39 NiCo/SiO₂-MOF catalyst exhibits the best catalytic performance for the hydrogenation of FA to
40 THFA, giving 99.8% conversion of FA and 99.1% selectivity to THFA. Significant synergistic
41 effect exists between Co and Ni within the subnanometer NiCo/SiO₂-MOF catalyst, which is
42 twice and 20 times more active than Ni/SiO₂-MOF and Co/SiO₂-MOF, respectively. In contrast,
43 such a synergistic effect is not observed within the NiCo/SiO₂-IMP catalyst prepared by
44 conventional impregnation. This interesting finding of size-dependent bimetallic synergetic
45
46
47
48
49
50
51
52
53
54
55
56
57
58
59
60

1
2
3 effect provides guidance for enhancing the activity of bimetallic catalysts. Considering the
4 diversity of MOFs, the method developed in this work can be easily extended to prepare other
5 high-performance subnanometer alloy-based catalysts, such as NiFe, NiZn and CoNiCu, with a
6 wide range of catalytic applications.
7
8
9
10
11
12

13 **AUTHOR INFORMATION**

14 **Corresponding Author**

15
16
17 *E-mail for T.W.: wangtf@tsinghua.edu.cn
18
19
20
21

22 **Author Contributions**

23
24 The manuscript was written through contributions of all authors. All authors have given approval
25 to the final version of the manuscript.
26
27
28

29 **Notes**

30
31 The authors declare no competing financial interest.
32
33
34

35 **ASSOCIATED CONTENT**

36 **Supporting Information.**

37
38 The Supporting Information is available free of charge via the Internet at <http://pubs.acs.org>.
39
40 SEM, N₂ adsorption-desorption isotherms and mesopore size distributions of the Ni-MOF/SiO₂
41 and Co-MOF/SiO₂ composites; TEM, XPS, N₂ adsorption-desorption isotherms and mesopore
42 size distribution of the Ni/SiO₂-MOF, Co/SiO₂-MOF and impregnation catalysts; Reusability of
43 the NiCo/SiO₂-MOF catalyst; XRD, HRTEM, HAADF-STEM and element mapping of the
44 used NiCo/SiO₂-MOF catalyst (PDF)
45
46
47
48
49
50
51
52
53
54
55
56
57
58
59
60

ACKNOWLEDGMENTS

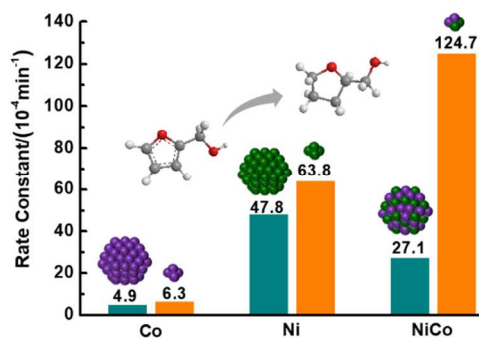
This work was financially supported by the National Natural Science Foundation of China (No. 21676155) and the PetroChina Innovation Foundation (No. 2016D-5007-0507).

REFERENCES

1. Li, X.; Jia, P.; Wang, T., *ACS Catal.* **2016**, *6*, 7621-7640.
2. Huber, G. W.; Iborra, S.; Corma, A., *Chem.Rev.* **2006**, *106*, 4044-4098.
3. Khan, F.-A.; Vallat, A.; Süss-Fink, G., *Catal. Commun.* **2011**, *12*, 1428-1431.
4. Lukes, R. M.; Nelson, L. S., *J. Org. Chem.* **1956**, *21*, 1096-1098.
5. Merat, N.; Godawa, C.; Gaset, A., *J. Chem. Tech. Biotechnol.* **1990**, *48*, 145-159.
6. Yuan, Q.; Ye, F.; Xue, T.; Guan, Y., *Appl. Catal. A* **2015**, *507*, 26-33.
7. Chen, X.; Sun, W.; Xiao, N.; Yan, Y.; Liu, S., *Chem. Eng. J.* **2007**, *126*, 5-11.
8. Tike, M. A.; Mahajani, V. V., *Ind. Eng. Chem. Res.* **2007**, *46*, 3275-3282.
9. King, G. M.; Iqbal, S.; Miedziak, P. J.; Brett, G. L.; SimonA.Kondrat; Yeo, B. R.; Liu, X.; Edwards, J. K.; Morgan, D. J.; Knight, D. K.; J.Hutchings, G., *ChemCatChem* **2015**, *7*, 21122-2129.
10. Hronec, M.; Fulajtárova, K.; Soták, T., *Appl. Catal. B: Environ.* **2014**, *154-155*, 294-300.
11. Iqbal, S.; Liu, X.; Aldosari, O. F.; Miedziak, P. J.; Edwards, J. K.; Brett, G. L.; Akram, A.; King, G. M.; Davies, T. E.; Morgan, D. J.; Knight, D. K.; Hutchings, G. J., *Catal. Sci. Technol.* **2014**, *4*, 2280-2286.
12. Zhang, B.; Zhu, Y.; Ding, G.; Zheng, H.; Li, Y., *Green Chem.* **2012**, *14*, 3402-3409.
13. Liu, H.; Huang, Z.; Zhao, F.; Cui, F.; Li, X.; Xia, C.; Chen, J., *Catal. Sci. Technol.* **2016**, *6*, 668-671.

- 1
2
3 14. Cao, Q.; Guan, J.; Peng, G.; Hou, T.; Zhou, J.; Mu, X., *Catal. Commun.* **2015**, 58, 76-79.
4
5 15. Koso, S.; Furikado, I.; Shima, A.; Miyazawa, T.; Kunimori, K.; Tomishige, K., *Chem.*
6
7 *Commun.* **2009**, 45, 2035-2037.
8
9
10 16. Koso, S.; Ueda, N.; Shinmi, Y.; Okumura, K.; Kizuka, T.; Tomishige, K., *J. Catal.* **2009**,
11
12 267, 89-92.
13
14 17. Pholjaroen, B.; Li, N.; Huang, Y.; Li, L.; Wang, A.; Zhang, T., *Catal. Today* **2015**, 245, 93-
15
16 99.
17
18 18. Gowda, A. S.; Parkin, S.; Ladipo, F. T., *Appl. Organomet. Chem.* **2012**, 26, 86-93.
19
20 19. Lee, J.; Farha, O. K.; Roberts, J.; Scheidt, K. A.; Nguyen, S. T.; Hupp, J. T., *Chem. Soc.*
21
22 *Rev.* **2009**, 38, 1450-1459.
23
24
25 20. Falcaro, P.; Ricco, R.; Yazdi, A.; Imaz, I.; Furukawa, S.; Maspooh, D.; Ameloot, R.; Evans,
26
27 J. D.; Doonan, C. J., *Coord. Chem. Rev.* **2016**, 307, 237-254.
28
29
30 21. Aijaz, A.; Fujiwara, N.; Xu, Q., *J. Am. Chem. Soc.* **2014**, 136, 6790-6793.
31
32 22. Chaikittisilp, W.; Hu, M.; Wang, H.; Huang, H. S.; Fujita, T.; Wu, K. C.; Chen, L. C.;
33
34 Yamauchi, Y.; Ariga, K., *Chem. Commun.* **2012**, 48, 7259-7261.
35
36
37 23. Chen, Y. Z.; Wang, C.; Wu, Z. Y.; Xiong, Y.; Xu, Q.; Yu, S. H.; Jiang, H. L., *Adv Mater*
38
39 **2015**, 27, 5010-5016.
40
41
42 24. Shen, K.; Chen, X.; Chen, J.; Li, Y., *ACS Catal.* **2016**, 6, 5887-5903.
43
44 25. Ma, T. Y.; Dai, S.; Jaroniec, M.; Qiao, S. Z., *J. Am. Chem. Soc.* **2014**, 136, 13925-31.
45
46
47 26. Jung, S.; Cho, W.; Lee, H. J.; Oh, M., *Angew. Chem. Int. Ed.* **2009**, 48, 1459-1462.
48
49 27. Shi, H.-Y.; Deng, B.; Zhong, S.-L.; Wang, L.; Xu, A.-W., *J. Mater. Chem.* **2011**, 21, 12309-
50
51 12315.
52
53
54
55
56
57
58
59
60

- 1
2
3 28. Kang, X.; Liu, H.; Hou, M.; Sun, X.; Han, H.; Jiang, T.; Zhang, Z.; Han, B., *Angew. Chem.*
4
5 **2016**, 128, 1092-1096.
6
7
8 29. Zhao, J.; Wang, F.; Su, P.; Li, M.; Chen, J.; Yang, Q.; Li, C., *J. Mater. Chem.* **2012**, 22,
9
10 13328-13333.
11
12 30. Li, H.; Liang, M.; Sun, W.; Wang, Y., *Adv. Funct. Mater.* **2016**, 26, 1098-1103.
13
14 31. Chen, S.; Xue, M.; Li, Y.; Pan, Y.; Zhu, L.; Qiu, S., *J. Mater. Chem. A* **2015**, 3, 20145-
15
16 20152.
17
18 32. Long, J.; Shen, K.; Chen, L.; Li, Y., *J. Mater. Chem. A* **2016**, 4, 10254-10262.
19
20 33. Yaghi, O. M.; Li, H.; Groy, T. L., *J. Am. Chem. Soc.* **1996**, 118, 9096-9101.
21
22 34. Zhu, L.-P.; Xiao, H.-M.; Fu, S.-Y., *Eur. J. Inorg. Chem.* **2007**, 2007, 3947-3951.
23
24 35. Biju, V., *Mater. Res. Bull.* **2007**, 42, 791-796.
25
26 36. Barrios, C. E.; Albiter, E.; Gracia y Jimenez, J. M.; Tiznado, H.; Romo-Herrera, J.; Zanella,
27
28 R., *Int. J. Hydrogen Energy* **2016**, 41, 23287-23300.
29
30 37. Chen, W.-T.; Chan, A.; Sun-Waterhouse, D.; Moriga, T.; Idriss, H.; Waterhouse, G. I. N., *J.*
31
32 *Catal.* **2015**, 326, 43-53.
33
34 38. Sexton, B. A.; Hughes, A. E.; Turney, T. W., *J. Catal.* **1986**, 97, 390-406.
35
36 39. Law, Y. T.; Dintzer, T.; Zafeiratos, S., *Appl. Surf. Sci.* **2011**, 258, 1480-1487.
37
38 40. Majumdar, D.; Spahn, R. G.; Gau, J. S., *J. Electrochem. Soc.* **1987**, 134, 1825-1829.
39
40 41. Hu, X.; Westerhof, R. J. M.; Dong, D.; Wu, L.; Li, C. Z., *ACS Sustainable Chem. Eng.*
41
42 **2014**, 2, 2562-2575.
43
44
45
46
47
48
49
50
51
52
53
54
55
56
57
58
59
60



For Table of Contents Only